Collagen and Leather

RESEARCH

Open Access

Development of mADM-collagen wound dressings for mimicking native skin architecture to enhance skin wound healing

Xiang Wang[1], Yujia Jiang[1], Xiaoqin Sun[1], Chongxia Yue[1,2*], Zhengyong Li[3*] and Yao Wu[1]

Abstract

Acellular dermal matrix (ADM) is one of the most promising scaffold materials due to its ability to retain natural extracellular matrix structure. Micronized acellular dermal matrix (mADM) was prepared with no intact cell nuclei and preserved growth factors by High Hydrostatic Pressure (HHP) approach. And mADM-collagen wound dressings were developed with different proportion of type I collagen and recombinant humanized type III collagen. The porous structure of the mADM-collagen wound dressings made them a good candidate for preventing excessive fluid accumulation, while the collagens with gel-like texture combined with mADM powder to form pasty texture wound dressing, which preserving the moisture at the wound site. Moreover, the paste texture of the mADM-collagen wound dressing was easy to reshape to conform any wound shapes and body contours. Furthermore, the resulted mADM-collagen wound dressings showed good biocompatibility by supporting fibroblasts adhesion and proliferation in vitro. Subsequently, a murine model of full-thickness skin wounds was employed to assess its effects on wound healing. Notably, mADM-75% Col-I exhibited superior effects throughout the wound healing process, specifically it promoted neovascularization, skin appendage growth and new skin regeneration. This formulation closely mimicked the collagen ratio found in healthy skin, facilitating the favorable wound repair. These results indicated the superior performance of this mADM-collagen wound dressing providing an optimal environment for wound healing.

Keywords mADM, Collagen, Wound dressings, Wound healing, Neovascularization

*Correspondence:
Chongxia Yue
yuechongxia@scu.edu.cn
Zhengyong Li
lizydd@wchscu.edu.cn
Full list of author information is available at the end of the article

Graphical Abstract

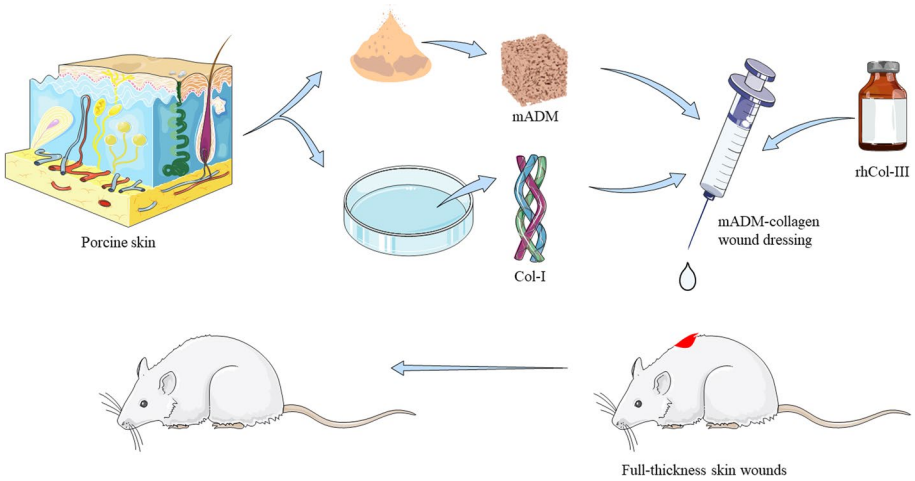

1 Introduction

Skin is the first defense barrier of the body which protects the body against damage and microbial invasion and provides the functions of thermoregulation, sensation and metabolism. Burns, mechanical trauma and diseases, lead to disruption of skin integrity and function [1, 2]. Wound management is an important issue in the medical system. Though skin has an extent of regenerating ability, chronic wounds resulted by diabetic, neurological disease, venous, and arterial ulcers are especially difficult to heal, which has become an important global medical problem [3].

An ideal wound dressing possesses several key properties that facilitate the wound healing process. First of all, maintaining an optimal moisture balance by retaining enough moisture to prevent drying out or excessive fluid accumulation at the wound site is one of the most important properties of wound dressings. Second, the wound dressing should be flexible to conform the wound shape, especially for the irregular wounds. Then, an ideal wound dressing should be biocompatible and can promote angiogenesis and granulation [4–6].

The extracellular matrix (ECM) plays vital roles in keeping the integrities of the tissues and organs by equipping them with a three-dimensional spatial structure and bioactive cytokines to facilitate multidirectional communications among various cells. Hence it is essential for maintaining tissue homeostasis [7, 8]. Acellular dermal matrix (ADM) is an ideal material for skin reconstruction, mimics the native dermis microenvironment, providing physical support to the skin and regulating cell function by controlling the biochemical gradients, cell density, spatial organization, and attachment ligands [9]. However, the presence of foreign cellular material and antigens could lead to adverse cell/host responses and thus requires the minimization/elimination of immunogenic risk before clinical applications [10]. Numerous decellularization methods have been developed for the removal of cellular and genetic materials while preserving extracellular matrix structure and bioactive composition. There are various decellularization methods including physical, chemical and enzymatic approaches. Chemical approaches are commonly employed for decellularization through the solubilization of cellular membranes, dissociation of DNA and disruption of lipid-protein interactions. Enzymes approaches target cellular and genetic materials removal by cleavage of cell–cell/ECM interactions and nucleic acids [11, 12]. Though chemical and enzymes approaches could remove cellular materials completely, they often adversely affect the critical ECM components and exhibit substantial cytotoxicity due to the chemical or biological residues [13]. Physical methods could effectively prevent disruption of ECM structure, which were incentivized to investigate physical method for decellularization. Akio Kishida et al. used high-hydrostatic pressure (HHP) technology to acquire decellularized blood vessels and cornea. HHP could disrupt cells, bacteria, and viruses in the tissue physically and then the residues of cellular components including lipids, proteins, and nucleic acids were removed by a washing process [14, 15]. It is generally believed that under the condition of ultrahigh pressure, the non-covalent bonding such as hydrogen bonding, hydrophobic bonding, ionic bonding and other non-covalent bonding

changes in the three-dimensional structure of macromolecules of organisms.

Micronized acellular dermal matrix (mADM) has been successfully used both in pre-clinical animal studies and in human clinical applications, which is able to remove cells and cellular components from a dermis and leave the natural mixture of structural and functional proteins that constitute the extracellular matrix, such as collagen, fibronectin, laminin and vimentin. Additionally, the mADM could be completely degraded, absorbed and readily turned over to produce new dermal tissue [16]. It exhibits excellent tissue compatibility, good mechanical properties, strong ability to promote normal tissue regeneration [17]. Collagen is one of the most important extracellular matrices, existing widely in connective tissues or organs [18, 19]. It is biodegradable, absorbable, non-toxic and biocompatible, and can provide support for cell attachment, migration and proliferation [20]. As wound dressings, collagen could absorb a large amount of exudate due to its ability of water absorption, reducing the loss of protein and electrolytes from traumatic exudate and avoiding dehydration of the wound [21]. Additionally, skin is mainly composed of type I and type III collagens maintaining the normal tissue structure of the skin [22].

In this study, a wound dressing without chemical or biological residues, simulating the skin extracellular matrix microenvironment was expected to be designed to promote wound repair and reduce scar formation. The novelty of the current work is the preparation of a skin regeneration template for accelerating full-layer skin defect wound healing using a new combination of mADM and type I collagen (Col-I) and recombinant humanized type III collagen (rhCol-III). It was suitable for shaping with more precise contour and irregular wound surface to avoid surgical incision and separation effectively. We investigated the efficiency of decellularization, physical and chemical properties of the material. The cytotoxicity of the mADM-collagen wound dressings and their ability to promote wound healing were evaluated in vitro and in vivo.

2 Materials & methods

2.1 Preparation of micronized acellular dermal matrix(mADM)

Porcine skin was subjected to a series of procedures to obtain 0.6 mm thick dermis. After cutting into 2×2 cm pieces, the dermal samples were degreased by dichloromethane (1 g/2 ml, Chron Chemicals, Sichuan, China) for 3 rounds of 30-min sonication. Then samples were freeze-dried for 48 h, ground to powder (50 − 250 μm), treated hypotonically in RO water for 24 h, subjected to repeated freeze–thaw three times in − 80 °C and underwent HHP treatment at 350 MPa for 30 min. Following this, the dermal matrix was washed in phosphate-buffered saline (PBS) for a period of 3 days and then freeze-dried. The obtained mADM was sterilized through irradiation before further experimentation.

2.2 Characterizations of mADM

Hematoxylin and eosin staining (H&E staining) was employed to visualize the presence of intact cell nuclei within mADM. Specifically, mADM samples were immobilized, dehydrated, paraffin-embedded, and sliced according to a standard protocol. Then, after H&E staining, microscopic observations were applied. Moreover, quantitative evaluation of epidermal growth factor (EGF), granulocyte–macrophage colony stimulating factor (GM-CSF) and platelet-derived growth factor (PDGF) in mADM were performed via enzyme-linked immunosorbent assay (ELISA) by Pig EGF ELISA Kit (Cusabio, HuBei, China), Porcine GM-CSF ELISA Kit (Neobioscience, Guangdong, China), Porcine PDGF-BB ELISA Kit (ColorfulGene, HuBei, China), respectively. The microstructure of mADM was observed using scanning electron microscopy (SEM), with native dermal powder serving as Control.

2.3 Preparation and characterizations of collagen

Col-I derived from porcine skin was prepared by ChipBio (SiChuan, China). Briefly, porcine skin was degreased by dichloromethane (1 g/2 ml) for 3 rounds of 30-min sonication at 4 °C. Then the resulted porcine skin was digested by pepsin (Aladdin Reagent, Shanghai, China) at pH 3.0 for 10-12 h. Subsequently, the type I collagen was collected and purified by centrifuged at 15000 g for 15 min and dialyzed with ultra-purified water until the conductivity of dialysate equal to ultra-purified water. The rhCol-III was purchased from Jland Biotech (70–90%, Batch No.: PA2180S003, Jiangsu, China). The amino acid sequence of rhCol-III was not disclosed for commercial reasons.

Sodium dodecyl sulfate polyacrylamide gel electrophoresis (SDS-PAGE) was used to identify the characteristic collagen peptide chains. Briefly, type I collagen or rhCol-III was mixed with sample buffer and heated at 100 °C for 5 min, and the resultant solution was loaded onto 5% (stacking) and 7.5% (running) polyacrylamide gels in a vertical slab (1 mm thick) for electrophoresis after centrifugation. After Coomassie bright blue dyeing and decolorization, gel images were captured using a ChemiDoc Imaging System (Bio-Rad, USA). Furthermore, fourier transform infrared (FT-IR, Nicolet 6700 spectrometer, PE, USA) was applied to investigate chemical bonds in type I collagen and rhCol-III at the wavelength of 4000–400 cm^{-1}. Circular

Dichroism (CD) was employed to assess the secondary structure of type I collagen and rhCol-III. Briefly, the collagen sample was loaded into the 1 mm path quartz pool, then wavelength scanning was performed in the range of 180–260 nm at 25 °C. Transmission electron microscope (TEM, Talos F200S, Thermo Scientific, USA) was used to examine the transverse structure of collagen fibers. SEM was applied to observe the microstructure of type I collagen and rhCol-III. The rhCol-III was qualitatively detected by adding tannic acid test solution (5%) with a molecular weight of 1701.20 to rhCol-III solution (0.1 mg/ml) and confirming the existence of white precipitate produced by tannic acid binding to the amino end of amino acids in collagen proteins.

2.4 Preparation and characterizations of mADM-collagen wound dressings

To prepare mADM-collagen wound dressings, 125 mg of mADM was combined with varying proportions of type I collagen and recombinant humanized type III collagen by a homogenizer, as specified in Table 1. The microstructure of mADM-collagen wound dressings was obtained by SEM analysis after immobilization, dehydration and lyophilization.

2.5 In vitro biocompatibility of mADM-collagen wound dressings

2.5.1 CCK-8 assay

Mouse fibroblasts (L929) were cultured with Dulbecco's Modified Eagle's Medium (DMEM, Gibco, USA) containing 10% fetal bovine serum (FBS, BI, ISR), and 1% antibiotics (HyClone, USA) and cultured at 37 °C with 5% CO_2. MADM-collagen wound dressings were placed in sterile 15 mL centrifugation tubes to prepare extracts by extracting with cell culture medium at 37 °C for 72 h. Then, 100 μL cell suspension containing 1×10^4 L929 cells was inoculated and cultured with sample extracts for 24 and 48 h. Cell media was replaced with fresh medium contained CCK-8 reagent after 24 h and 48 h incubation, and optical density (OD) was measured at 450 nm after incubation at 37 °C for another 2 h. The cells cultured without extracts were used as negative control.

Table 1 Composition of mADM-collagen wound dressing

mADM	125 mg mADM
mADM-Col-I	125 mg mADM + 1 mL Col-I
mADM-75%Col-I	125 mg mADM + 0.75 mL Col-I + 0.25 mL rh Col-III
mADM-75%Col-III	125 mg mADM + 0.25 mL Col-I + 0.75 mL rh Col-III

2.5.2 Cell morphology

MADM-collagen wound dressings were placed at the bottom of cell culture dish and incubated with 1 ml DMEM at 37 °C for 1 h to form gel. Then 1 mL of cell suspension containing 2×10^4 L929 cells was added and cultured for 1d, 3d, 5d and 7d. Cell morphology was observed by confocal laser scanning microscopy (CLSM, LSM880 ZISS, Germany) after staining with Phalloidin-TRITC (beyotime, China) and 4′,6-diamidino-2-phenylindole (DAPI, beyotime, China).

2.5.3 Cell viability

Briefly, 1 mL of cell suspension containing 1×10^5 L929 cells was cultured with mADM-collagen wound dressings for 1 and 3 days. Then, live/dead staining was applied to observe cell viability under CLSM.

2.6 In vivo study

2.6.1 Surgical procedure for full-thickness wound in rats

There were 16 healthy 7-weeks old male SD rats included in this study. Full-thickness skin wounds were created on the back of rats, in which 12 of rats were received mADM-collagen wound dressings while the remaining 4 were served as sham surgical controls. Briefly, the animals were anesthetized with Zoletil and wounds were established on the rats' back after shaving and general disinfection. Then, different mADM-collagen wound dressings were applied on the wounds and bandaged with gauze. Wound healing progress was monitored by taking photographs on the 3rd, 7th, and 14th days post-operation.

2.6.2 Tissue processing, histological and immunohistochemical analysis

On the 3rd, 7th and 14th day post-operation, the required tissues were processed with standard protocol including fixation, dehydration, paraffin embedding and section with Leica RM2255 microtome. Tissue sections were stained with H&E staining and Masson's Trichrome staining to analyze the regenerated dermis and collagen deposition of healing wounds. Immunohistochemical analysis of TGF-β3, Smad7, TGF-BRII, CD31 and α-SMA was conducted on the 7th day post-operation. Finally, the Halo software was performed to evaluate vascularization of wound healing and thickness of regenerated dermis in H&E staining images and was used to quantify the density of all the immunohistochemical images.

2.7 Statistics

Data were presented as mean ± standard deviation. Statistical significance was assessed using one-way analysis of variance (ANOVA) with GraphPad Prism 8 software (GraphPad Software Inc., USA). Significance level was denoted as (*) $p < 0.05$, (**) $p < 0.01$ and (***) $p < 0.001$ respectively. P values < 0.05 were considered statistically significant.

3 Results & discussion

3.1 Decellularization by high hydrostatic pressurization

Acellular dermal matrix (ADM), three-dimensional natural biomaterials, was harvested by removal of cellular components without altering intrinsic structure, morphology and composition of the extracellular matrix [23]. It exhibited excellent tissue compatibility, good mechanical properties, low absorption rate, strong ability to promote normal tissue regeneration [17]. In our study, we employed freeze–thaw cycling and high hydrostatic pressure for decellularization, such physical approaches led to good biocompatibilities of the resulted mADM due to no chemical residues and providing a large surface area for cell adhesion and growth and facilitating the transport of nutrients and oxygen through interconnected pores [24]. The efficacy of decellularization of mADM was evaluated through H&E staining (Fig. 1A), in which no intact cell nuclei in mADM observed, indicating complete cell removal. Moreover, the collagen fibrils were slightly loosened in mADM after decellularization as compared to the native porcine skin (Control). In order to further

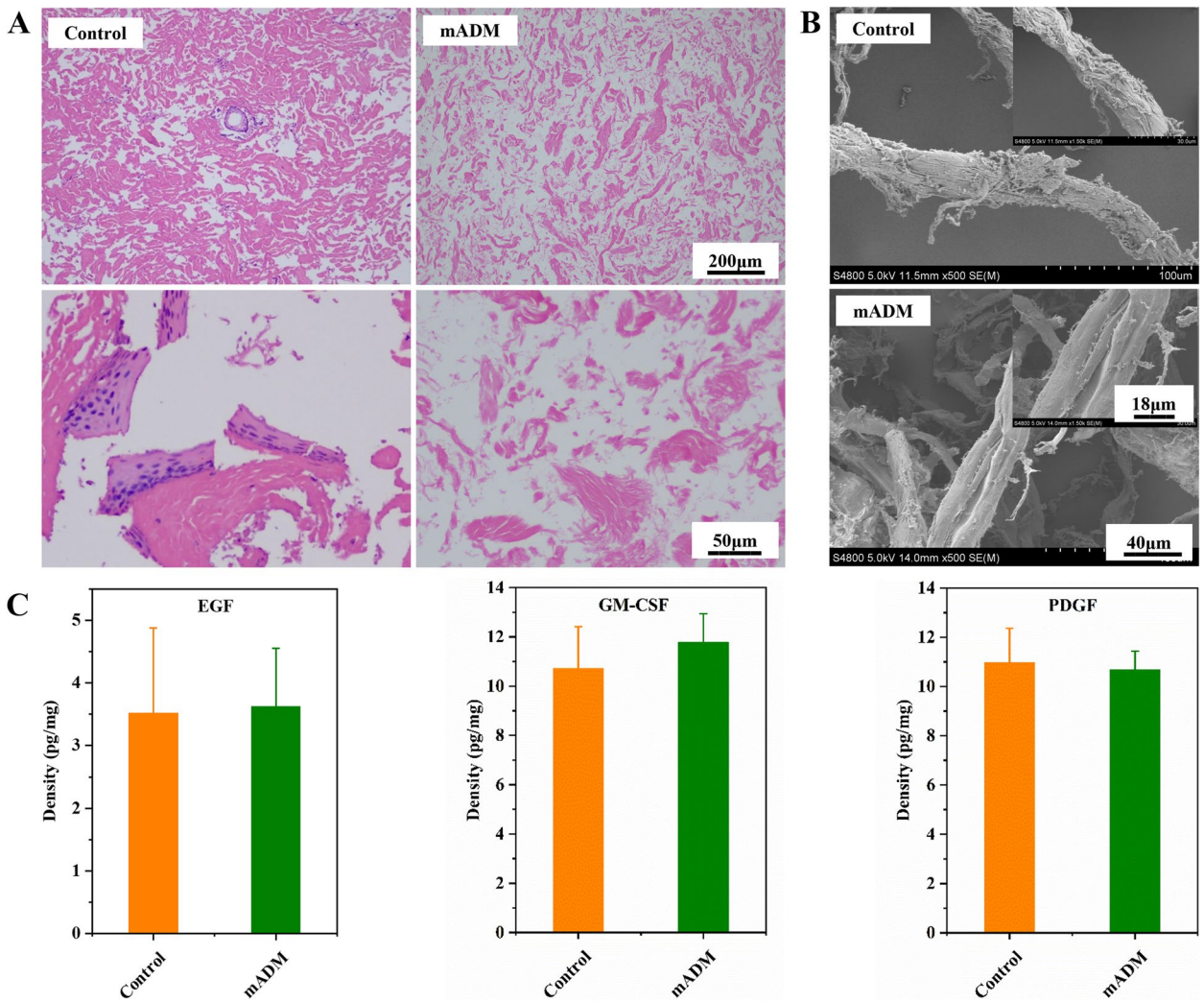

Fig. 1 Decellularization and growth factors retaining of mADM. **A** Representative H&E staining of native dermal matrix (Control) and mADM. No intact cell nucleus after decellularization. **B** SEM images of Control and mADM, with smooth surface of mADM. **C** Density of EGF, GM-CSF and PDGF remaining displayed no significant difference between Control and mADM

explore structural difference, SEM was used to observe the microstructure of mADM and Control (Fig. 1B). There was no significant difference in the width of collagen fiber bundles when comparing mADM with Control, though mADM showed relatively smoother surface in SEM images with more fine smooth collagen fibers. Bioactive growth factors also contributed to accelerate wound healing. Hence, we tested the concentrations of EGF, GM-CSF and PDGF in mADM. Specifically, GM-CSF is one of the most widely studied cytokines in wound healing, which influences the activity of keratinocytes and fibroblasts and increases the production of vascular endothelial growth factor [25, 26]. EGF increases the migration and proliferation of keratinocytes which plays a vital role in the epithelialization process [27]. Moreover, PDGF increases collagen production by fibroblasts and promotes angiogenesis by stimulating endothelial migration [28, 29]. All the tested growth factors in mADM were comparable to those in native porcine skin, as shown in Fig. 1C, which significantly impact several stages of wound healing. In summary, our approach effectively removed cellular substances while preserving growth factors like EGF, GM-CSF, and PDGF at high level, critical for wound healing, which is often a challenge with other decellularization approaches [30].

3.2 Characterizations of collagen

The FT-IR pattern of bovine standard Col-I, type I collagen and rhCol-III was shown in Fig. 2A, which identified their characteristic peaks and validated their composition. The bovine standard Col-I and Col-I sample showed same absorption patterns. The N–H stretching vibration and the coupling of hydrogen bonds produced an amide A band and an amide B band at 3307.5 cm^{-1} and 2939.2 cm^{-1}, respectively. The absorption peak at 1633.5 cm^{-1} was the amide I band, proved bovine standard Col-I, type I collagen and rhCol-III have typical hydrogen bonds for collagen formed by the recurrent N–H···O=C [31]. The absorption peak at 1548.6 cm^{-1} and 1238.1 cm^{-1} were the amide II band and amide III band of collagen respectively. The FT-IR pattern of rhCol-III showed similar absorption peaks with bovine standard Col-I and Col-I though with lower peak values, which indicated that the rhCol-III and Col-I had similar secondary structure, however, the difference of amino acid contents might be a reason for forming different interchain interactions [32].

The circular dichroic chromatography was used to analyze the protein tertiary structure of bovine standard Col-I, type I collagen and rhCol-III. As shown in Fig. 2B, both type I collagen sample and bovine standard Col-I

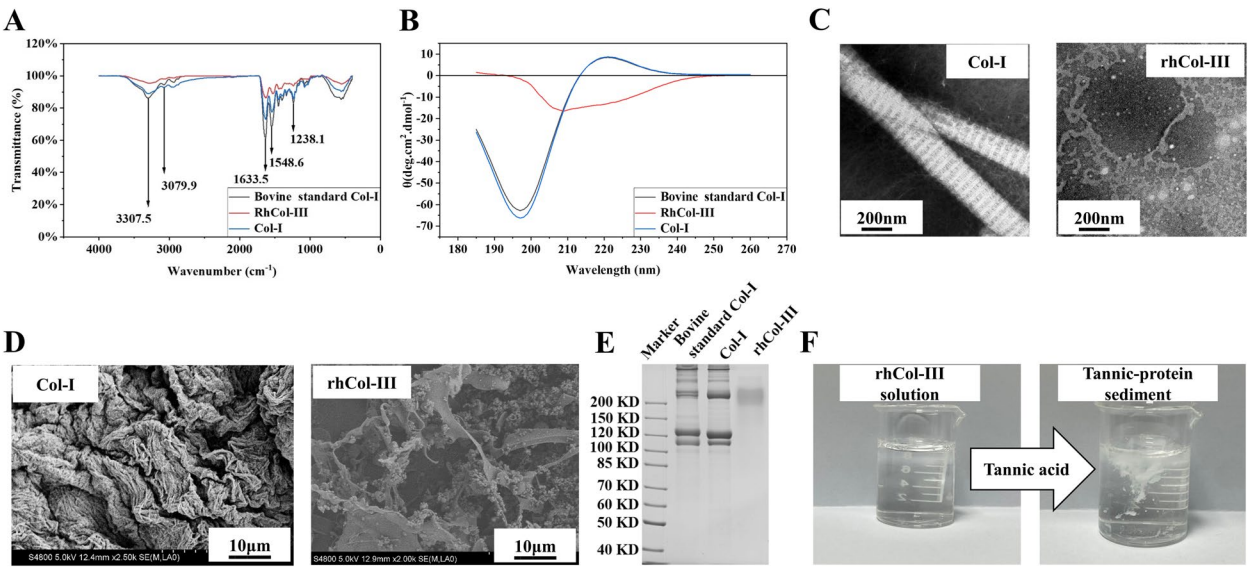

Fig. 2 Characterizations of type I and the recombinant humanized type III collagen. **A** FT-IR of type I collagen, bovine standard Col-I and rhCol-III revealed peaks at 3307.5 cm^{-1}, 2939.2 cm^{-1}, 1633.5 cm^{-1}, 1548.6 cm^{-1} and 1238.1 cm^{-1}, corresponding to the amide A band, the amide B band, the amide I band, the amide II band and the amide III band, respectively, consistent with accepted collagen analysis. **B** CD mapping of type I collagen and bovine standard Col-I showed no significant difference, while rhCol-III showed no positive absorption peak. **C** TEM of type I collagen fibers showed typical light and dark stripe with about 67 nm spacing structure with 200 nm in width, while rhCol-III was a structure of wafers. **D** SEM of type I collagen and recombinant humanized type III collagen. **E** SDS-PAGE analysis of type I collagen (lane 3) was similar to bovine standard Col-I (lane 2) and typical bands were confirmed in type I collagen, while rhCol-III (lane 3) had only one diffused band between 190–210 KD. **F** Qualitative detection of the recombinant humanized type III collagen solution tested by tannic acid solution. White sediment appeared immediately after the addition of tannic acid to rhCol-III water solution

had a strong negative absorption peak at 197 nm and a positive absorption peak at 221 nm, in which the negative absorption peak was caused by the π-π amide bond transition and the positive absorption peak was caused by the n-π amide bond transition. While the rhCol-III showed no positive absorption peak, which indicated no typical triple helix structure in rhCol-III. The ratio of the positive absorption peak to the peak of the negative absorption peak of type I collagen sample and standard was about 0.13. These results confirmed the integrity of the triple helix structure of collagen in both type I collagen sample and bovine standard Col-I. As shown in Fig. 2E, type I collagen (lane 3) and bovine standard Col-I (lane 2) exhibited similar bands. Bands at 100 KD, 116 KD, 205 KD and 295 KD were corresponded to the α1, α2, β and γ chains of collagen respectively. For rhCol-III, a diffused band was observed between 190–210 KD. TEM images (Fig. 2C) depicted the typical light and dark stripe with about 67 nm spacing structure of type I collagen fibers with 200 nm in width, while rhCol-III was a structure of wafers [33]. SEM images (Fig. 2D) showed that rhCol-III was mixture of flakes and fine fibers and Col-I were coarse fibers formed by interweaving fine fibers. The results of TEM confirmed the existence of typical triple helix structure in Col-I.

Tannic acid can bind to the amino end of amino acids in proteins, causing protein denaturation and precipitation. Therefore, tannic acid could be used for the qualitative detection of the recombinant humanized type III collagen (Fig. 2F). The type III collagen solution was clear without precipitation after full dissolution. When drops of the tannic acid test solution were added, the solution immediately became cloudy and produced white precipitate.

3.3 Characterizations of mADM-collagen wound dressings

In the present study, we have combined mADM with type I collagen and recombinant humanized type III collagen with different portion to form such an ideal wound dressing.

Figure 3A showed that mADM-Col-I and mADM-75% Col-I presented pasty substance at room temperature, while mADM-75% Col-III displayed a more fluid texture. The recombinant humanized type III collagen existed in a solution form, whereas the type I collagen exhibited a gel-like texture. Consequently, as the proportion of rhCol-III increased in the wound dressings, it enhanced the mobility of the materials. The resulting dressings exhibited remarkable flexibility, enabling easy coverage of irregular wounds. Furthermore, the microstructure of mADM-collagen dressings was observed by SEM (Fig. 3B). The presence of coarse mADM fibers in all three mADM-collagen wound dressings provided a framework for cell adhesion and proliferation. In comparison to mADM-75% Col-III, the structures in mADM-Col-I and mADM-75% Col-I were denser. The porous structure of the resulted mADM-collagen wound dressings as evidenced by SEM results made them a good candidate for preventing excessive fluid accumulation, while the pasty texture wound dressing, which preserved the moisture at the wound site.

3.4 In vitro study of cytocompatibility

3.4.1 Cell viability of L929 on the mADM-collagen wound dressings

To further investigate cell viability on the wound dressings, we performed live/dead fluorescence staining of L929 cells after culturing them on different wound dressings for 1 and 3 days (Fig. 3C). The number of live cells (green) on all the wound dressings increased over the culturing period, indicating good cell viability on all the wound dressings.

3.4.2 Cytotoxicity of mADM-collagen wound dressings

To evaluate the cytotoxicity of the mADM-collagen wound dressings, L929 cells were co-cultured with extracts of different wound dressings for 24 h and 48 h. The cell viability of L929 cells in mADM-Col-I, mADM-75% Col-I and mADM-75% Col-III groups were significantly higher than the only mADM group. Moreover, the cell viability of all the wound dressings increased with incubation time (Fig. 3D).

3.4.3 Cell morphology of L929 on the mADM-collagen wound dressings

Cytoskeleton and nucleus staining of L929 cells were observed after co-culturing with mADM-collagen wound dressings (Fig. 3E). The cells maintained a round shape on all the mADM-collagen wound dressings. Nonetheless, the cells were significantly proliferated over the culturing period. As shown in Fig. 3E, there was little adherent cells on all the wound dressings at day 1, yet the number of adherent cells increased steadily during the co-culturing period.

The resulted mADM-collagen wound dressing in our study showed good biocompatibility by supporting fibroblasts adhesion and proliferation in vitro. Collagen dressings increased fibroblast production and uptake, contributed to fibronectin absorption and bioavailability, assisted the retention of leukocytes, macrophages, fibroblasts, and epithelial cells, as well as preservation of wound tissue [34].

3.5 In vivo wound healing examinations

3.5.1 Wound observation

The mADM and mADM-collagen wound dressings were applied to the full-thickness wounds, which

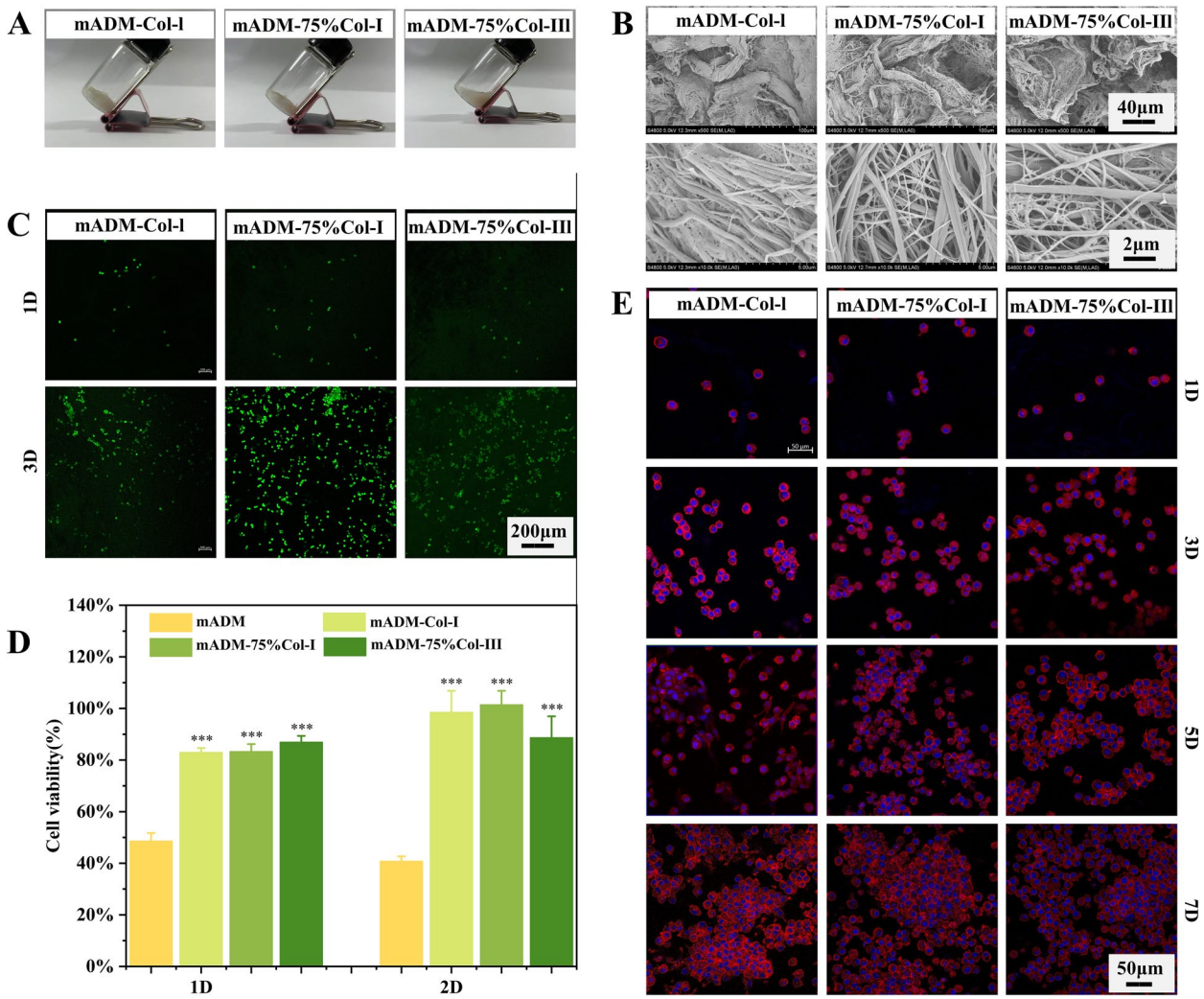

Fig. 3 Morphology, microstructure and biocompatibility evaluation of mADM-collagen wound dressings. **A** Morphology of mADM-collagen wound dressings at room temperature. mADM-75% Col-III showed a more viscous fluid texture while others presented a pasty shape. **B** SEM images of mADM-collagen wound dressings. The addition of rhCol-III led to an increase in fine fibers and a subsequent loosening of the structure in the mADM-collagen wound dressing. **C** Live/Dead staining of L929 cells cultured with mADM-collagen wound dressings for 1 and 3 days. The number of live cells (green) increased with incubation time. **D** CCK-8 assays showed that the cell viability of L929 cells cultured with mADM-collagen wound dressings extracts were significantly higher than the only mADM group. **E** Cell morphology over 1, 3, 5, and 7 days, stained by Phalloidin-TRITC and DAPI, displayed consistent round cell shapes with steady proliferation

could easily attach to the wound surface (Fig. 4A). The group without any treatment was set as Control. Figure 4B showed the wound healing progress of the rats over the healing period. Three days post-operation, the wounds of the Control group exhibited crusting, while the wounds of the wound dressing groups retained the dressing materials. Despite similar wound sizes across all groups initially, notable differences emerged during the healing process. Seven days post-surgery, the mADM, mADM-Col-I, mADM-75%Col-I and mADM-75%Col-III showed significantly smaller wound size, which were 5.3 ± 0.4 mm, 5.1 ± 0.9 mm, 6.5 ± 1.0 mm and 4.2 ± 1.1 mm, respectively. While the Control group with the wound size of 8 ± 1.4 mm. By the 14th day, the wound dressing groups displayed completed wound repair, while the Control group exhibited persistent blood scabs. The mADM-collagen groups had smaller wound area than the Control groups and showed no blood scar, expressing faster wound repair. The result indicated the superior performance of this mADM-Collagen wound dressing, providing an optimal environment for wound healing [35].

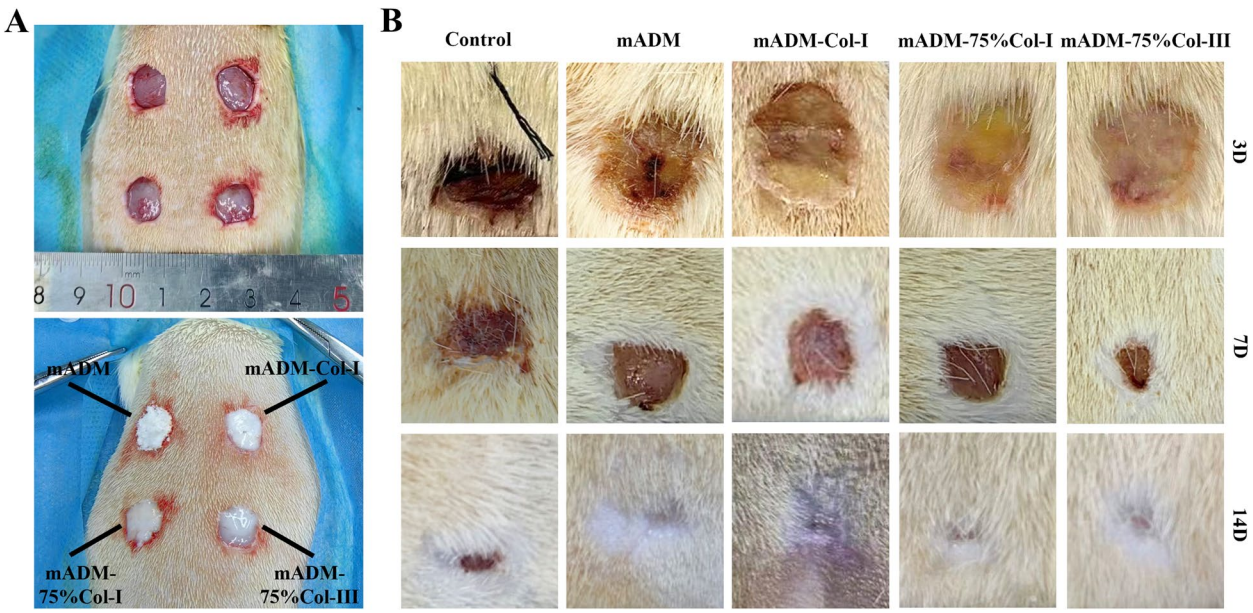

Fig. 4 Observation of wound healing. **A** Representative images of the establishment of full-thickness wounds and the application of mADM-collagen wound dressings. **B** Images of the wounds progression over the healing period. The wound dressing groups showed smaller wound area (5.5 ± 1.5 mm) than that of Control groups (8 ± 1.4 mm) at the 7th day. Blood scarring was still visible in the Control groups at the 14th day

3.5.2 H&E staining and Masson's trichrome staining

In order to explore the internal regeneration process of the newborn tissue, wound tissue was sectioned for H&E and Masson's trichrome staining at each designed time point.

Generally, H&E staining revealed the presence of growing skin appendages in the mADM-collagen wound dressing groups (Fig. 5A), while the Masson staining indicated no significant difference in collagen deposition among all groups (Fig. 5B). The amount of collagen deposition was increased steadily over the wound healing period. A large number of inflammatory cells gathered along the wound site in all groups at 3 days post-operation. After 7 days, the thickness of the regenerated dermis increased in all groups, accompanied by the dispersion of inflammatory cells throughout the regenerated tissue. The number and distribution of inflammatory cells in the mADM-collagen wound dressing groups indicated that all of them had good biocompatibility, and no stimulation effect on local tissue, evidenced by no sign of accumulation of inflammation cells. Hair follicles and their attached sebaceous glands were equivalent to the relevant components of reconstructed skin [36]. By the 14th day, notable growing of skin appendages was observed in the mADM-collagen wound dressing groups. Specifically, mADM-Col-I group displayed the emergence of hair follicles and sebaceous glands, while only hair follicle structures was observed in mADM-75% Col-I group. Additionally, the mADM-75% Col-III group demonstrated appendage-like tissue formation. In contrast, minimal skin appendages were observed in both mADM and Control groups, indicating that the mADM-collagen wound dressings significantly stimulated skin appendage growth. Furthermore, the regenerated skin of mADM and mADM-collagen group at the 14th day was thicker than Control group, while the mADM-75% Col-I group showed significant difference (Fig. 5D). Revascularization was an essential part of granulation tissue, because blood vessels could transport oxygen and nutrients to the wound sites and served as a template for the formation of new dermis [37, 38]. Evaluation of vascular density at 3, 7 and 14 days post-operation indicated that the mADM-collagen wound dressing groups promoted vascularization during the early stages of wound healing, while the number of blood vessels in the Control group was significantly higher than the mADM group and all the mADM-collagen wound dressing groups at 14 days post-operation (Fig. 5C). It might be because type I and III collagen are able to bind to platelet receptors, then activate platelet adhesion and aggregation and initiate the clotting pathway which promoted blood vessel development [39].

3.5.3 Immunohistochemical analysis

Figure 6A, B displayed immunohistochemical analysis of the wound tissues at the 7th day, the mADM group and all the mADM-collagen wound dressing groups exhibited

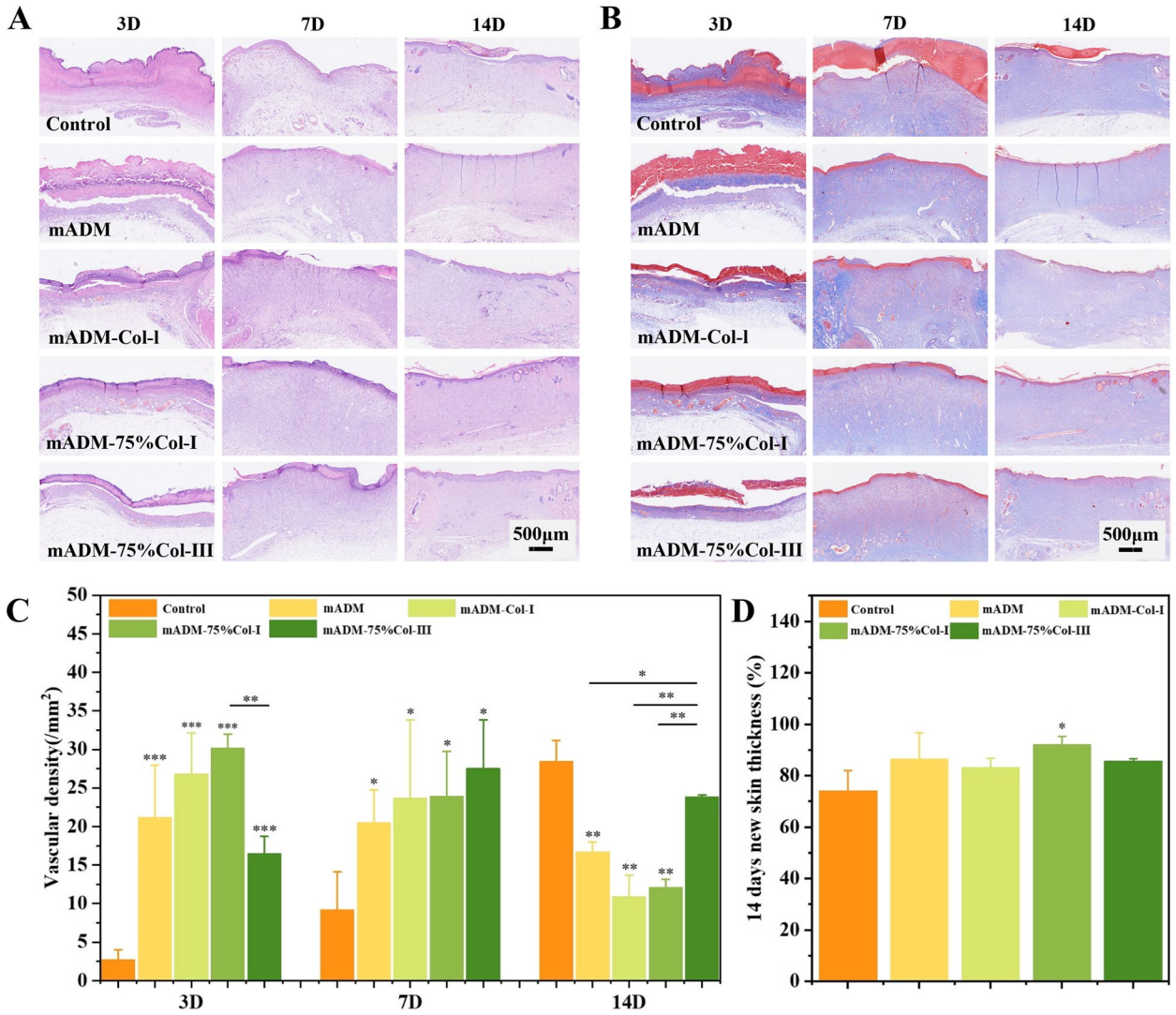

Fig. 5 Histological analysis of wound healing: **A** H&E staining revealed the presence of growing skin appendages in the mADM-collagen wound dressing groups. **B** Masson staining indicated no significant difference in collagen deposition among all groups. **C** Evaluation of vascular density at 3, 7, 14 days post-operation indicated that the mADM-collagen wound dressing groups promoted vascularization during the early stages of wound healing. **D** Thickness of the regenerated skin assessment indicated that mADM-75% Col-I exhibited the most effective repairing effect

a higher CD31 expression compared to the Control group, indicating increased vascularization in the experimental set, though no significant difference was found. Conversely, Fig. 6C depicted a significantly lower expression of α-SMA, a marker expressed in abnormal scar, in the mADM-75% Col-I group when compared to other groups [40]. It is reported that excessive type I and III collagen would promote scar formation [41, 42]. Therefore the type I and III collagen ratio in mADM-75% Col-I group probably had the effect of avoiding scar formation as compared to the other mADM-collagen wound dressings in the present study. Additionally, TGF-β promoted re-epithelialization, granulation tissue formation, and increased collagen deposition by stimulating fibroblasts into the wound site, which was expected to be important for efficient wound healing. In the study, the expressions of Smad7, TGF-βRII, and TGF-β3 was showed in Fig. 6D-F and no significant differences were observed among all groups.

During the mADM-collagen groups, mADM-75% Col-I showed the best wound repair effect at early and late stage. Collagen I and III represent the most common collagen components in skin tissue with the deposition ratio of collagen type I and III tightly related to skin regeneration. Type III collagen is the first type of collagen produced during embryonic development and during the

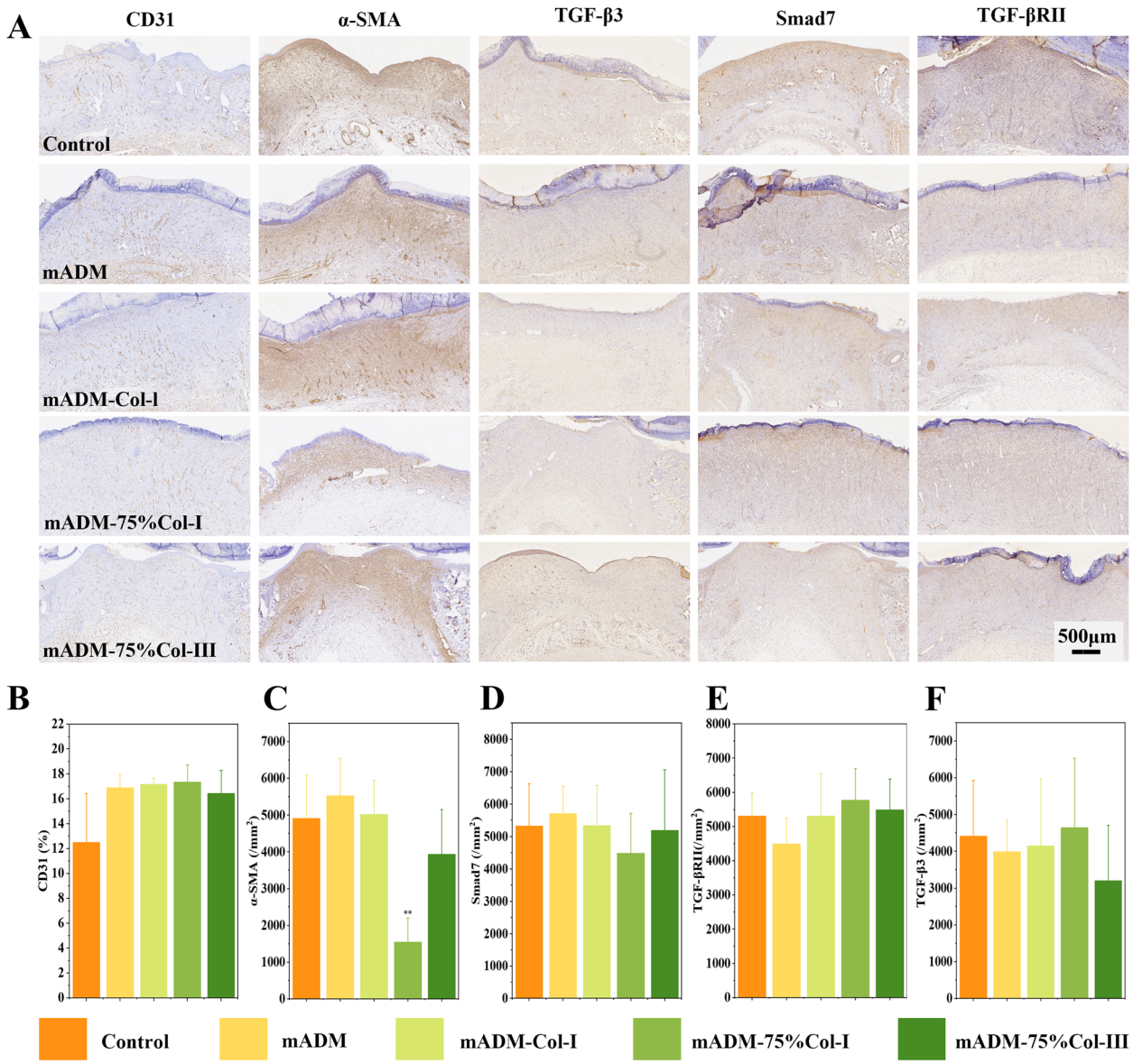

Fig. 6 **A** Immunohistochemical staining images for CD31, α-SMA, Smad7, TGF-β3 and TGF-βRII in skin wounds at the 7th day after operation. **B**-**F** Quantification of mean density of CD31, α-SMA, Smad7 and TGF-βRII and TGF-β3, respectively

early phase of wound healing. In humans, the fetal dermis is comprised of about 20% of type III collagen while adult dermis contains about 10% [43]. The ratio between collagen I/III in the mADM-75% Col-I groups was closed to the healthy skin, which may lead the superior wound healing effects [44].

Notably, mADM-75% Col-I exhibited superior effects throughout the wound healing process. This formulation closely mimicked the collagen ratio found in healthy skin, facilitating the favorable wound repair. Thus mADM-75% Col-I emerged as a promising wound dressing candidate for efficient wound healing.

4 Conclusion

In conclusion, we developed mADM-collagen wound dressings with different proportion of type I collagen and recombinant humanized type III collagen. Among these, the mADM-75% Col-I dressing closely mimicked dermal architecture significantly enhanced wound healing. In vitro assessments highlighted that mADM-collagen wound dressings support cellular functions and proliferation. While in vivo experiments confirmed their role in promoting neovascularization, skin appendage growth, and new skin regeneration without eliciting immune responses. The mADM-75% Col-I dressing

emerges as a promising wound dressing for rapid wound healing. However, the rhCol-III with different amino acid sequence and structure could be an important parameter to affect the wound repairing effects of the final wound dressing which needs further study. And the signal pathways of how mADM-Collagen wound dressings repairing human skin should be further studied.

Abbreviations

ADM	Acellular dermal matrix
CD	Circular dichroism
CLSM	Confocal laser scanning microscopy
Col-I	Type I collagen
DAPI	4′,6-Diamidino-2-phenylindole
ECM	Extracellular matrix
EGF	Epidermal growth factor
ELISA	Enzyme-linked immuno-sorbent assay
FBS	Fetal bovine serum
FT-IR	Fourier transform infrared
GM-CSF	Granulocyte–macrophage colony stimulating factor
H&E staining	Hematoxylin and eosin staining
HHP	High-hydrostatic pressure
L929	Mouse fibroblasts
mADM	Micronized acellular dermal matrix
OD	Optical density
PBS	Phosphate-buffered saline
PDGF	Platelet-derived growth factor
rhCol-III	Recombinant humanized type III collagen
SDS-PAGE	Sodium dodecyl sulfate polyacrylamide gel electrophoresis
SEM	Scanning electron microscopy
TEM	Transmission electron microscope

Supplementary Information

The online version contains supplementary material available at https://doi.org/10.1186/s42825-024-00159-5.

Supplementary Material 1.

Acknowledgements
Not applicable.

Authors' contributions
XW: Writing, experiments. YJJ: Data analysis. XQS: Manuscript modification. CXY: Manuscript modification, supervision, organization of the experiment, the funding. ZYL: Manuscript modification, supervision, resources. YW: Supervision, organization of the experiment, the funding and resources.

Funding
This work was supported by the National Natural Science Foundation of China (Grant Nos. 31971265, 32271397, 31971257); National Key Research and Development Program of China (Grant No. 2022YFC2406102); Major Project of Sichuan Science and Technology Department (Grant No. 2022ZDZX0029-1); and the Medical Device Regulatory Scientific Research Center Innovation Team Cultivation Project (SCU2023YLQX).

Availability of data and materials
All data generated or analyzed during this study are included in this published article.

Declarations

Ethics approval and consent to participate
All animal studies were approved by The Institutional Animal Care and Use Committee of Sichuan University (Chengdu, China, K2023026). All animals were purchased from DaShuo experimental animal Co. Ltd. (Chengdu, China).

Consent for publication
The Author confirms that the work described has not been published before; that it is not under consideration for publication elsewhere; that its publication has been approved by all co-authors; that its publication has been approved (tacitly or explicitly) by the responsible authorities at the institution where the work is carried out.

Competing interests
The authors declare that they have no competing interests.

Author details
[1]College of Biomedical Engineering/National Engineering Research Center for Biomaterials, Sichuan University, Chengdu, People's Republic of China. [2]NMPA Key Laboratory for Quality Research and Control of Tissue Regenerative Biomaterial & Institute of Regulatory Science for Medical Devices & NMPA Research Base of Regulatory Science for Medical Devices, Sichuan University, Chengdu, People's Republic of China. [3]Department of Burn and Plastic Surgery, West China Hospital, Sichuan University, Chengdu, People's Republic of China.

Received: 21 December 2023 Revised: 20 March 2024 Accepted: 26 March 2024
Published online: 01 July 2024

References

1. Zhang Y, Jiang W, Kong L, Fu J, Zhang Q, Liu H. PLGA@IL-8 nanoparticles-loaded acellular dermal matrix as a delivery system for exogenous MSCs in diabetic wound healing. Int J Biol Macromol. 2023;224:688–98.
2. Goodarzi P, Falahzadeh K, Nematizadeh M, Farazandeh P, Payab M,Larijani B, Tayanloo Beik A, Arjmand B. Tissue engineered skin substitutes. Adv Exp Med Biol. 2018;1107:143–88.
3. Xiao H, Chen X, Liu X, Wen G, Yu Y. Recent advances in decellularized biomaterials for wound healing. Mater Today Bio. 2023;19:100589.
4. Peng W, Li D, Dai K, Wang Y, Song P, Li H, Tang P, Zhang Z, Li Z, Zhou Y, Zhou C. Recent progress of collagen, chitosan, alginate and other hydrogels in skin repair and wound dressing applications. Int J Biol Macromol. 2022;208:400–8.
5. Nicholas MN, Jeschke MG, Amini-Nik S. Methodologies in creating skin substitutes. Cell Mol Life Sci. 2016;73(18):3453–72.
6. Aljghami ME, Saboor S, Amini-Nik S. Emerging innovative wound dressings. Ann Biomed Eng. 2018;47(3):659–75.
7. Nyström A, Bruckner-Tuderman L. Matrix molecules and skin biology. Semin Cell Dev Biol. 2019;89:136–46.
8. Walraven M, Hinz B. Therapeutic approaches to control tissue repair and fibrosis: extracellular matrix as a game changer. Matrix Biol. 2018;71–72:205–24.
9. Reing JE, Brown BN, Daly KA, Freund JM, Gilbert TW, Hsiong SX, Huber A, Kullas KE, Tottey S, Wolf MT, Badylak SF. The effects of processing methods upon mechanical and biologic properties of porcine dermal extracellular matrix scaffolds. Biomaterials. 2010;31(33):8626–33.
10. Wong ML, Griffiths LG. Immunogenicity in xenogeneic scaffold generation: antigen removal vs. decellularization. Acta Biomater. 2014;10(5):1806–16.
11. Yang D, Fang Z, Kang R, Liu K. Composite electrospun scaffold containing decellularized amniotic matrix for pelvic organ prolapse. Mater Des. 2021;210:110106.
12. Wang B, Qinglai T, Yang Q, Li M, Zeng S, Yang X, Xiao Z, Tong X, Lei L, Li S. Functional acellular matrix for tissue repair. Mater Today Bio. 2023;18:100530.
13. Zhao J, Yu W, Zhang Q, Li X, Huang Y, Zhao S, Li T, Liu S, Li Y, Shan H. Structural and biofunctional evaluation of decellularized jellyfish matrices. J Mater Chem B. 2023;11(16):3740–51.
14. Funamoto S, Nam K, Kimura T, Murakoshi A, Hashimoto Y, Niwaya K, Kitamura S, Fujisato T, Kishida A. The use of high-hydrostatic pressure treatment to decellularize blood vessels. Biomaterials. 2010;31(13):3590–5.
15. Hashimoto Y, Funamoto S, Sasaki S, Honda T, Hattori S, Nam K, Kimura T, Mochizuki M, Fujisato T, Kobayashi H, Kishida A. Preparation and characterization of decellularized cornea using high-hydrostatic pressurization for corneal tissue engineering. Biomaterials. 2010;31(14):3941–8.

16. Chu J, Shi P, Deng X, Jin Y, Liu H, Chen M, Han X, Liu H. Dynamic multiphoton imaging of acellular dermal matrix scaffolds seeded with mesenchymal stem cells in diabetic wound healing. J Biophotonics. 2018;11:e201700336.
17. Kulig KM, Luo X, Finkelstein EB, Liu X-H, Goldman SM, Sundback CA, Vacanti JP, Neville CM. Biologic properties of surgical scaffold materials derived from dermal ECM. Biomaterials. 2013;34(23):5776–84.
18. Sun L, Li L, Wang Y, Li M, Xu S, Zhang C. A collagen-based bi-layered composite dressing for accelerated wound healing. J Tissue Viability. 2022;31(1):180–9.
19. Chaudhari A, Vig K, Baganizi D, Sahu R, Dixit S, Dennis V, Singh S, Pillai S. Future prospects for scaffolding methods and biomaterials in skin tissue engineering: a review. Int J Mol Sci. 2016;17(12):1974.
20. Tang P, Song P, Peng Z, Zhang B, Gui X, Wang Y, Liao X, Chen Z, Zhang Z, Fan Y, Li Z, Cen Y, Zhou C. Chondrocyte-laden GelMA hydrogel combined with 3D printed PLA scaffolds for auricle regeneration. Mater Sci Eng C. 2021;130:112423.
21. Cui B, Zhang C, Gan B, Liu W, Liang J, Fan Z, Wen Y, Yang Y, Peng X, Zhou Y. Collagen-tussah silk fibroin hybrid scaffolds loaded with bone mesenchymal stem cells promote skin wound repair in rats. Mater Sci Eng C. 2020;109:110611.
22. Cheng W, Yanhua R, Yuming S, Guoan Z. Contents and ratios of type I and type III collagens in normal skin and hypertrophic scar in people of different ages. J Shandong Univ (Health Sciences). 2016;54:64–7.
23 Carvalho-Júnior JDC, Zanata F, Aloise AC, Ferreira LM. Acellular dermal matrix in skin wound healing in rabbits - histological and histomorphometric analyses. Clinics. 2021;76:e2066.
24. Zhang X, Deng Z, Wang H, Yang Z, Guo W, Li Y, Ma D, Yu C, Zhang Y, Jin Y. Expansion and delivery of human fibroblasts on micronized acellular dermal matrix for skin regeneration. Biomaterials. 2009;30(14):2666–74.
25. Cruciani M, Lipsky BA, Mengoli C, Lalla FD. Are granulocyte colony-stimulating factors beneficial in treating diabetic foot infections? A meta-analysis. Diabetes Care. 2005;28(2):454–60.
26. Castro-Dopico T, Fleming A, Dennison TW, Ferdinand JR, Harcourt K, Stewart BJ, Cader Z, Tuong ZK, Jing C, Lok LSC, Mathews RJ, Portet A, Kaser A, Clare S, Clatworthy MR. GM-CSF calibrates macrophage defense and wound healing programs during intestinal infection and inflammation. Cell Rep. 2020;32(1):107857.
27. Tahir T, Febrianti N, Wahyuni S, Rabia, Syam Y. Evaluation of acute wound healing potential of red dragon fruit (Hylocereus Polyrhizus) extract cream on type III collagen and Epidermal Growth Factor (EGF) levels: an animal study. Med Clín Práct. 2020;3:100091.
28. Parhizkari N, Eidi M, Mahdavi-Ortakand M, Ebrahimi-kia Y, Zarei S, Pazoki Z. The effect of oral treatment of royal jelly on the expression of the PDGF-β gene in the skin wound of male mice. J Tissue Viability. 2023;32(4):536–40.
29. Lai F, Dai S, Zhao Y, Sun Y. Combination of PDGF-BB and adipose-derived stem cells accelerated wound healing through modulating PTEN/AKT pathway. Injury. 2023;54(6):1451–61.
30. Crapo PM, Gilbert TW, Badylak SF. An overview of tissue and whole organ decellularization processes. Biomaterials. 2011;32(12):3233–43.
31. Boryskina OP, et al. Energies of peptide–peptide and peptide–water hydrogen bonds in collagen: evidences from infrared spectroscopy, quartz piezogravimetry and differential scanning calorimetry. J Mol Struct. 2007;827(1–3):1–10.
32. Wang J, et al. Characterization of recombinant humanized collagen type III and its influence on cell behavior and phenotype. J Leather Sci Eng. 2022;4:33.
33. Gibney R, Patterson J, Ferraris E. High-resolution bioprinting of recombinant human collagen type III. Polymers. 2021;13(17):2973.
34. Pasaribu KM, Ilyas S, Tamrin T, Radecka I, Swingler S, Gupta A, Stamboulis AG, Gea S. Bioactive bacterial cellulose wound dressings for burns with collagen in-situ and chitosan ex-situ impregnation. Int J Biol Macromol. 2023;230:123118.
35. Baldursson BT, Kjartansson H, Konrádsdóttir F, Gudnason P, Sigurjonsson GF, Lund SH. Healing rate and autoimmune safety of full-thickness wounds treated with fish skin acellular dermal matrix versus porcine small-intestine submucosa. Int J Low Extrem Wounds. 2015;14(1):37–43.
36. Chen L, Huang C, Zhong Y, Chen Y, Zhang H, Zheng Z, Jiang Z, Wei X, Peng Y, Huang L, Niu L, Gao Y, Ma J, Yang L. Multifunctional sponge scaffold loaded with concentrated growth factors for promoting wound healing. iScience. 2023;26(1):105835.
37. Gong M, Shi H, Hu Z, Wang F, Dong M, Lei R, Zeng Z, Wang Y, Chen J. Aerogel-hydrogel biphase gels based on physically crosslinked β-lactoglobulin fibrils/polyvinyl alcohol for skin wound dressings: in vitro and in vivo characterization. Chem Eng J. 2023;473:145394.
38. Chen L, Ma J, Chen Y, Huang C, Zheng Z, Gao Y, Jiang Z, Wei X, Peng Y, Yu S, Yang L. Polydopamine modified acellular dermal matrix sponge scaffold loaded with a-FGF: promoting wound healing of autologous skin grafts. Biomater Adv. 2022;136:212790.
39. Manon-Jensen T, Kjeld NG, Karsdal MA. Collagen-mediated hemostasis. J Thromb Haemost. 2016;14(3):438–48.
40. Limandjaja GC, Belien JM, Scheper RJ, Niessen FB, Gibbs S. Hypertrophic and keloid scars fail to progress from the CD34−/α-smooth muscle actin (α-SMA)+ immature scar phenotype and show gradient differences in α-SMA and p16 expression. Br J Dermatol. 2020;182(4):974–86.
41. Arima T, Uchiyama M, Nakano Y, et al. Peroxisome proliferator-activated receptor alpha agonist suppresses neovascularization by reducing both vascular endothelial growth factor and angiopoietin-2 in corneal alkali burn. Sci Rep. 2017;7:17763.
42. Kim H-y, Im H-y, Chang H-k, Jeong H-d, Park J-h, Kim H-i, Yi H-s, Kim Y-s. Correlation between collagen type I/III ratio and scar formation in patients undergoing immediate reconstruction with the round block technique after breast-conserving surgery. Biomedicines. 2023;11(4):1089.
43. Smith LT, Holbrook KA, Madr JA. Collagen types I, III, and V in human embryonic and fetal skin. Am J Anat. 1986;175:507–21. https://doi.org/10.1002/aja.1001750409.
44. Cameron AM, Turner CT, Adams DH, Jackson JE, Melville E, Arkell RM, Anderson PJ, Cowin AJ. Flightless I is a key regulator of the fibroproliferative process in hypertrophic scarring and a target for a novel antiscarring therapy. Br J Dermatol. 2016;174(4):786–94.

Publisher's Note